FETI-based Homogenization of Composites with Perfect Bonding and Debonding of Constituents

Pavel Gruber

***Abstract*—The present paper deals with the homogenization of composite materials with periodic microstructure. Emphasis is put on mathematical modeling of imperfect bonding between linearly elastic constituents. Elements of homogenization theory are introduced, together with the Unit Cell problem governing the macroscopic response of the equivalent homogeneous body. Numerical resolution of mathematical and physical problem of homogenization is based on the Finite Element Tearing and Interconnecting (FETI) method, extended to cover both cases of the perfect bonding and debonding of individual constituents. It is demonstrated that FETI allows very efficient treatment of the conventional homogenization problem for composites with the limit zero as well as infinite values of interfacial compliance. Verification of the method is performed using selected data available in open literature.**

***Index Terms*—contact problem, composites, debonding, FETI, homogenization, imperfect bonding of constituents, modified conjugate gradient method, unit cell**

I. Introduction

IN THIS work, we focus on a problem of finding homogenized properties for a cross-section of composite materials with long fibers in the state of plane stress or plane strain. Composites with periodic microstructure with perfect and imperfect bonding of constituents are considered. Attention is paid to the behavior of interfaces between the matrix phase and fibers, and to the case of pre-existing and load-induced debonding phenomena in particular. Note that the introduced theory can be naturally extended to treat more general interfacial constitutive laws, such as compliant interfaces with a limited ductility [4], [6].

The rest of the paper is organized as follows. Section II deals with the homogenization of the composites with periodic microstructure and linearly elastic constituents in the range of small displacements and strains. Additional details on the homogenization of composite materials with periodic microstructure can be found, e.g., in a review article [7] or in a diploma thesis [4]. In Section III, we employ the principle of minimum potential energy – the Lagrange variational principle – to solve the homogenization problem. The Finite Element Tearing and Interconnecting method, see e.g. [5] for a recent review, is employed to discretize the problem in terms of nodal displacements and nodal forces. Following recent non-traditional extensions of the FETI algorithm [3], [6], [9], we propose a simple approach to the incorporation of perfect bonding as well as load-induced and pre-existing debonding phenomena. Finally, representative set of numerical experiments performed in MATLAB is presented Section IV to demonstrate the efficiency of the proposed scheme. Additional examples and more detailed discussion can be found in the diploma thesis [4].

P. Gruber is with the Department of Mechanics, Faculty of Civil Engineering, Czech Technical University in Prague, Thákurova 7, 166 29 Prague 6, Czech Republic, email: pavel.gruber@centrum.cz

Supported by research project GAČR 106/08/1379 and GAČR 106/07/1244

II. Homogenization

In the present context, the homogenization of a composite sample is understood as the replacement of a heterogeneous material by a certain homogeneous equivalent, which delivers the identical mechanical response. As noted in the previous Section, we focus on the composites with periodic microstructure and perfect and imperfect interfaces between the matrix and fibers.

A. Unit cell

The key notion of the theory of homogenization of periodic composites is a unit cell ($\mathcal{UC}$) – a part of the composite, which, if repeated periodically, generates the analyzed microstructure. Clearly, the choice of the unit cell is non-unique and is typically motivated by the numerical resolution of the unit cell problem, mainly by the geometrical and material symmetries and by the application of the periodic boundary conditions. For these reasons, the rectangular $\mathcal{UC}$s are typically employed.

We assume in the sequel that a $\mathcal{UC}$ occupies a domain $\Omega^{\mathcal{UC}} \subset \mathbb{E}^2$ with a boundary $\Gamma^{\mathcal{UC}}$. Next, we denote $\Omega^{\mathcal{C}}$ and $\Gamma^{\mathcal{C}}$ the domains of the composite body and the boundary of a composite, respectively; see Fig. 1 for an illustration.

B. Macro and micro scale

Consider first a composite sample taken from a homogeneous material on the macroscale. On this level we introduce a macroscopic strain tensor $\mathbf{E}(\mathbf{x})$ and a macroscopic stress $\mathbf{\Sigma}(\mathbf{x})$. Vector $\mathbf{x}$ determines the location of a point on the relevant scale.

The next level – the microscale – refers to the level of resolution where the individual constituents of a composite can be recognized. Vector $\mathbf{y}$ will be used to determine a location of a point on this scale and the micro-stress and micro-strain fields are denoted by $\boldsymbol{\epsilon}(\mathbf{y})$ and $\boldsymbol{\sigma}(\mathbf{y})$, respectively. Both possible views of the composite, including the introduced notation, are depicted in Fig. 1.

C. Strain approach to homogenization

In the adopted approach to computation homogenization, an unknown macroscopic stress field $\mathbf{\Sigma}(\mathbf{x})$ is determined from a known macroscopic strain field $\mathbf{E}(\mathbf{x})$; i.e. we employ the strain-controlled homogenization [7]. This particular choice

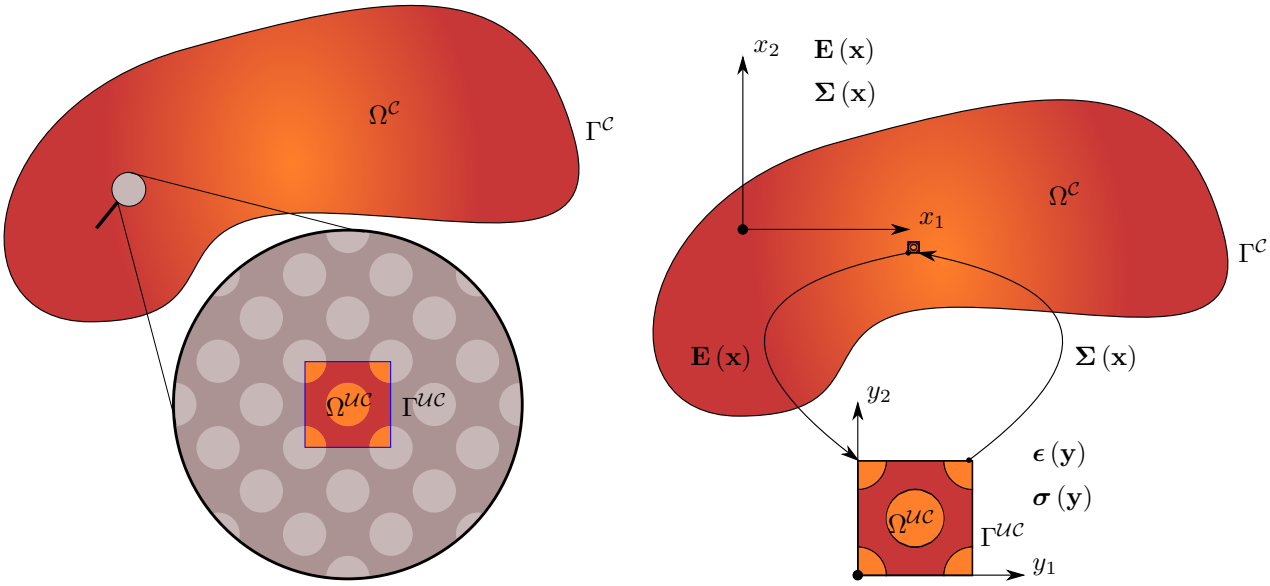

Fig. 1. Principle of homogenization.

can be formally postulated with the help of the density of macroscopically stored deformation energy $W(\mathbf{E}(\mathbf{x}))$ as

$$\mathbf{\Sigma}(\mathbf{x}) = \frac{\partial W(\mathbf{E}(\mathbf{x}))}{\partial \mathbf{E}(\mathbf{x})}. \tag{1}$$

Such an approach is analogous to the deformation method of the traditional theory of elasticity.

The principle of the strain-controlled approach to the homogenization is clearly visible from Fig. 1. In particular, the macrostrain from a point $\mathbf{x}$ loads the corresponding $\mathcal{UC}$ and the interaction with neighboring $\mathcal{UC}$s enforces suitable boundary conditions on $\Gamma^{\mathcal{UC}}$, resulting in the local unit cell problem. Of course, the boundary conditions can not be chosen arbitrarily in order to preserve a correct macro-micro transfer of the stress field, the strain field and the stored energy.

D. Consistency conditions

The consistency conditions ensure the same average behavior on the both scales, since both levels ought to deliver the same effective response. It follows that the macroscopic strain $\mathbf{E}(\mathbf{x})$ and the macroscopic stress $\mathbf{\Sigma}(\mathbf{x})$ at a point of macroscale $\mathbf{x}$ must be, in a certain way, identical to the microscopic strain $\boldsymbol{\epsilon}(\mathbf{y})$ and strain fields $\boldsymbol{\sigma}(\mathbf{y})$ on the corresponding domain $\Omega^{\mathcal{UC}}$ on the microscale, respectively.

To than end, let $\langle f(\mathbf{y})\rangle$ denote the spatial average of a function $f(\mathbf{y})$ on a domain Ω defined as

$$\langle f(\mathbf{y})\rangle = \frac{1}{|\Omega|}\int_{\Omega} f(\mathbf{y})\,\mathrm{d}\Omega, \tag{2}$$

where $|\Omega|$ denotes the area a domain $\Omega \subset \mathbb{E}^2$. Then, the consistency of the strain and the stress fields is satisfied iff

$$\langle \boldsymbol{\epsilon}(\mathbf{y})\rangle = \mathbf{E}(\mathbf{x}) \quad \wedge \quad \langle \boldsymbol{\sigma}(\mathbf{y})\rangle = \mathbf{\Sigma}(\mathbf{x}), \tag{3}$$

$$\forall \mathbf{y} \in \Omega^{\mathcal{UC}}, \quad \forall \mathbf{x} \in \Omega^{\mathcal{C}}. \tag{4}$$

Note that the previous relations can be interpreted as generalized kinematic and static boundary conditions.

E. Strain fields consistency

Because we aim to solve the local problem (the boundary-value problem for a given macroscopic strain $\mathbf{E}(\mathbf{x})$) by the help of the displacement-based methods, the microscopic strain field $\boldsymbol{\epsilon}(\mathbf{y})$ is considered to be the primary unknown. Consequently, we must impose special requirements on the microscopic strain field $\boldsymbol{\epsilon}(\mathbf{y})$ to enforce the consistency conditions (3).

For convenience, we decompose the microscopic strain field $\boldsymbol{\epsilon}(\mathbf{y})$ on the domain $\Omega^{\mathcal{UC}}$, corresponding to the macroscopic point $\mathbf{x}$, to two components:

$$\boldsymbol{\epsilon}(\mathbf{y}) = \mathbf{E}(\mathbf{x}) + \boldsymbol{\epsilon}^*(\mathbf{y}), \quad \forall \mathbf{y} \in \Omega^{\mathcal{UC}}, \tag{5}$$

where $\boldsymbol{\epsilon}^*(\mathbf{y})$ stands for the so-called fluctuating strain field accounting for the presence of heterogeneities. By analogy, we also introduce a similar decomposition of the microscopic stress field $\boldsymbol{\sigma}(\mathbf{y})$ and the field of displacements $\mathbf{u}(\mathbf{y})$. Using the Gauss-Green theorem, it can be shown that the identity

$$\langle \boldsymbol{\epsilon}^*(\mathbf{y})\rangle = \frac{1}{|\Omega^{\mathcal{UC}}|}\oint_{\Gamma^{\mathcal{UC}}} \mathbf{u}^* \otimes \mathbf{n}^{\mathcal{UC}}\,\mathrm{d}\Gamma^{\mathcal{UC}} = \mathbf{0}, \tag{6}$$

where

$$\mathbf{a} \otimes \mathbf{b} = \frac{1}{2}(a_i b_j + a_j b_i) \tag{7}$$

is equivalent to the strain consistency condition (3). Note that the symbol $\mathbf{n}^{\mathcal{UC}}$ appearing in the previous relation denotes the outer normal vector to the boundary of $\Omega^{\mathcal{UC}}$.

F. Stress fields consistency

In the framework of the strain-based homogenization, the micro-macro stress consistency can satisfied in a rather straightforward way. Once the micro-strain field $\boldsymbol{\epsilon}(\mathbf{y})$ is known, the stress field $\boldsymbol{\sigma}(\mathbf{y})$ follows from the constitutive equations and the stress equivalence condition (3) is automatically verified by averaging the micro-stress field on the domain $\Omega^{\mathcal{UC}}$.

G. Energetic condition – Hill's lemma

The last requirement of the correct micro-macro scale transfer is an energetic consistency condition – the Hill lemma, which requires that the average of the internal work on the microscale $\langle \boldsymbol{\sigma}(\mathbf{y}) : \boldsymbol{\epsilon}(\mathbf{y}) \rangle$ and internal work in the corresponding point on the macroscale $\boldsymbol{\Sigma}(\mathbf{x}):\mathbf{E}(\mathbf{x})$ must be identical:

$$\boldsymbol{\Sigma} : \mathbf{E} = \langle \boldsymbol{\sigma} : \boldsymbol{\epsilon} \rangle, \tag{8}$$

where

$$\mathbf{a} : \mathbf{b} = a_{ij} b_{ij}. \tag{9}$$

Similarly to Section II-E, it be proved that the energetic condition (8) can be ensured via an equivalent identity, cf. [7]:

$$\langle \boldsymbol{\sigma} : \boldsymbol{\epsilon}^* \rangle = \frac{1}{|\Omega^{\mathcal{UC}}|} \oint_{\Gamma^{\mathcal{UC}}} \boldsymbol{\sigma} \cdot \mathbf{n}^{\Omega^{\mathcal{UC}}} \cdot \mathbf{u}^* \, \mathrm{d}\Gamma^{\mathcal{UC}} = 0, \tag{10}$$

where

$$\mathbf{a} \cdot \mathbf{b} = a_i b_i. \tag{11}$$

H. Boundary conditions

If follows from relations (6) and (10) that the two-scale consistency can be imposed via appropriate boundary conditions formulated in the terms of the fluctuating displacement field $\mathbf{u}^*$ and the stresses $\boldsymbol{\sigma}(\mathbf{y})$ (or, more precisely, the boundary tractions). The particularly convenient choice are the so-called periodic kinematic and the so-called anti-periodic static boundary conditions on the boundary $\Gamma^{\mathcal{UC}}$, not only because they satisfy relations (6) and (10), but because they also reflect the assumed periodic distribution of the constituents in the composite body.

To describe the boundary conditions more formally, we denote the parts of the boundary parallel to the directions of invariance of the unit cell as $\Gamma^{\mathcal{UC}}_{\#1}$ and $\Gamma^{\mathcal{UC}}_{\#2}$, respectively. Any point $\mathbf{y}^{\#1}$ can be identified with a point $\mathbf{y}^{\#2}$ located on the homologous part of the boundary. The periodic kinematic and the anti-periodic static boundary conditions can then be stated as

$$\mathbf{u}^*\left(\mathbf{y}^{\#1}\right) = \mathbf{u}^*\left(\mathbf{y}^{\#2}\right) \quad \wedge \quad \mathbf{n}^{\Omega^{\mathcal{UC}}}\left(\mathbf{y}^{\#1}\right) = -\mathbf{n}^{\Omega^{\mathcal{UC}}}\left(\mathbf{y}^{\#2}\right)$$

and

$$\boldsymbol{\sigma}^*\left(\mathbf{y}^{\#1}\right) \cdot \mathbf{n}^{\Omega^{\mathcal{UC}}}\left(\mathbf{y}^{\#1}\right) = -\boldsymbol{\sigma}^*\left(\mathbf{y}^{\#2}\right) \cdot \mathbf{n}^{\Omega^{\mathcal{UC}}}\left(\mathbf{y}^{\#2}\right),$$

for every $(\mathbf{y}^{\#1}, \mathbf{y}^{\#2}) \in \Gamma^{\mathcal{UC}}_{\#1} \times \Gamma^{\mathcal{UC}}_{\#2}$.

III. FETI

In this section, we introduce fundamentals of solving the local problem of homogenization using the FETI method [3], [5], interpreted as an extended principle of minimum potential energy – the Lagrange variational principle, e.g. [2]. Note that in the rest of this paper, the Voigt notation (see e.g. [1]) is used instead of tensorial one.

A. Energetic functional

Consider a heterogeneous elastic body occupying the domain $\Omega^{\mathcal{UC}}$ in the Euclidean space $\mathbb{E}^2$ with the boundary $\Gamma^{\mathcal{UC}}$. The matrix phase is assumed to occupy the domain Ω^1 with the boundary Γ^1 and r fibers occupy the domains Ω^q with boundaries Γ^q, $q = 2, 3, ..., r+1$, satisfying

$$\overline{\Omega^{\mathcal{UC}}} = \bigcup_{q=1}^{r+1} \overline{\Omega^q} \quad \wedge \quad \Omega^t \cap \Omega^s = \emptyset, \quad \text{for } t \neq s. \tag{12}$$

Next, the $\mathcal{UC}$ is understood as a system of $(r+1)$ independent solid deformable bodies in $\mathbb{E}^2$ (r fibers and one matrix). We say that a boundary Γ^q belongs to a domain Ω^q if its outer normal $\mathbf{n}^q(\mathbf{y})$ points out of this domain.

The macroscopic strain $\mathbf{E}(\mathbf{x})$ loads the individual $\mathcal{UC}$ constituents (recall Fig.1) and surface tractions $\boldsymbol{\mu}(\mathbf{y})$, resulting from the compatibility of the displacement fields, load the individual boundaries Γ^g of the components. The surface tractions arise from two sources: (i) requirement the identical displacements between the neighboring constituents and (ii) the conditions of the stress anti-periodicity. The corresponding energy functional can be then written in the form:

$$\begin{aligned} \Pi(\mathbf{u}, \boldsymbol{\mu}) &= \frac{1}{2} \sum_{q=1}^{r+1} \int_{\Omega^q} \boldsymbol{\sigma}^{\mathrm{T}} \boldsymbol{\epsilon} \, \mathrm{d}\Omega^q \\ &+ \int_{\Gamma^1} \boldsymbol{\mu}^{\mathrm{T}} \mathbf{u} \, \mathrm{d}\Gamma^1 - \sum_{q=2}^{r+1} \int_{\Gamma^q} \boldsymbol{\mu}^{\mathrm{T}} \mathbf{u} \, \mathrm{d}\Gamma^q, \\ &\forall \{\mathbf{u}, \boldsymbol{\mu}\} \in \mathcal{D}_\Pi, \end{aligned} \tag{13}$$

where $\mathcal{D}_\Pi$ denotes the set of admissible displacement fields and boundary tractions.

Following Section II-E, the admissible displacements can be expressed as

$$\mathbf{u}(\mathbf{y}) = \mathbf{E}\mathbf{y} + \mathbf{u}^*(\mathbf{y}), \tag{14}$$

where $\mathbf{u}^*$ is a $\mathcal{UC}$-periodic displacement field. Because the periodic boundary conditions on $\mathbf{u}^*$ do not prevent the rigid body motions of $\mathcal{UC}$, additional boundary conditions need to be introduced. In our case, we use the Dirichlet boundary conditions:

$$\mathbf{u}^*(\mathbf{y}) = \mathbf{0}, \quad \forall \mathbf{y} \in \Gamma^{\mathcal{UC}}_D, \tag{15}$$

where $\Gamma^{\mathcal{UC}}_D$ corresponds to the corners of $\mathcal{UC}$. The next component of $\mathcal{D}_\Pi$ contains a field of the surface tractions $\boldsymbol{\mu}(\mathbf{y})$.[1] Altogether, we can write

$$\begin{aligned} \mathcal{D}_\Pi &= \left\{\mathbf{u}(\mathbf{y}) = \mathbf{E}\mathbf{y} + \mathbf{u}^*(\mathbf{y}), \quad \forall \mathbf{y} \in \Omega^{\mathcal{UC}}\right\} \\ &\cap \left\{\mathbf{u}^*(\mathbf{y}) = \mathbf{0}, \quad \forall \mathbf{y} \in \Gamma^{\mathcal{UC}}_D\right\} \\ &\cap \left\{\mathbf{u}^*(\mathbf{y}) \text{ periodic}, \quad \forall \mathbf{y} \in \Gamma^{\mathcal{UC}}\right\} \\ &\times \left\{\boldsymbol{\mu}(\mathbf{y}), \quad \forall \mathbf{y} \in \Gamma^q, \; q = 1, 2, \ldots, r+1\right\}. \end{aligned} \tag{16}$$

Introducing the Hooke law in the form, e.g. [1],

$$\boldsymbol{\sigma} = \mathbf{L}\boldsymbol{\epsilon}, \tag{17}$$

[1] Note that we do not impose any constraints on the values of the tractions, since we limit them in the outer loop of the incremental algorithm described in Section III-F. An alternative approach, derived from the mathematical programming methods, can be found in [3], [9].

where $\mathbf{L}(\mathbf{y})$ denote the stiffness matrix of a linear elastic material, and employing the decomposition of the microscopic strain field $\boldsymbol{\epsilon}(\mathbf{y})$ introduced in Eq. (5), the energy functional can be expressed in the form

$$\begin{aligned}\Pi &= \frac{1}{2}\sum_{q=1}^{r+1}\int_{\Omega^q}\left(\mathbf{E}^{\mathrm{T}}\mathbf{L}\mathbf{E}+2\mathbf{E}^{\mathrm{T}}\mathbf{L}\boldsymbol{\epsilon}^{*}+\boldsymbol{\epsilon}^{*\mathrm{T}}\mathbf{L}\boldsymbol{\epsilon}^{*}\right)\mathrm{d}\Omega^q \\ &+ \int_{\Gamma^1}\boldsymbol{\mu}^{\mathrm{T}}\left(\mathbf{E}\mathbf{y}+\mathbf{u}^{*}\right)\mathrm{d}\Gamma^1 \\ &- \sum_{q=2}^{r+1}\int_{\Gamma^q}\boldsymbol{\mu}^{\mathrm{T}}\left(\mathbf{E}\mathbf{y}+\mathbf{u}^{*}\right)\mathrm{d}\Gamma^q, \forall\{\mathbf{u},\boldsymbol{\mu}\}\in\mathcal{D}_{\Pi}, \quad (18)\end{aligned}$$

which appears to be more suitable for the further treatment.

B. Minimization problem

Observe that the macroscopic strain $\mathbf{E}(\mathbf{x})$ appearing in the functional (18) is constant for a given state of loading, the stiffness matrix $\mathbf{L}(\mathbf{y})$ is independent of the displacements $\mathbf{u}(\mathbf{y})$ and tractions $\boldsymbol{\mu}(\mathbf{y})$ and

$$\int_{\Gamma^1}\boldsymbol{\mu}^{\mathrm{T}}\mathbf{E}\mathbf{y}\,\mathrm{d}\Gamma^1=\sum_{q=2}^{r+1}\int_{\Gamma^q}\boldsymbol{\mu}^{\mathrm{T}}\mathbf{E}\mathbf{y}\,\mathrm{d}\Gamma^q. \quad (19)$$

Therefore, the only independent fields are the fluctuating displacements $\mathbf{u}^{*}(\mathbf{y})$ and surface tractions $\boldsymbol{\mu}(\mathbf{y})$ and the minimization problem can be recast into an equivalent form

$$\begin{aligned}\min_{\mathbf{u}^{*},\boldsymbol{\mu}}\Theta &= \frac{1}{2}\sum_{q=1}^{r+1}\int_{\Omega^q}\left(2\mathbf{E}^{\mathrm{T}}\mathbf{L}\boldsymbol{\epsilon}^{*}+\boldsymbol{\epsilon}^{*\mathrm{T}}\mathbf{L}\boldsymbol{\epsilon}^{*}\right)\mathrm{d}\Omega^q \\ &+ \int_{\Gamma^1}\boldsymbol{\mu}^{\mathrm{T}}\mathbf{u}^{*}\,\mathrm{d}\Gamma^1-\sum_{q=2}^{r+1}\int_{\Gamma^q}\boldsymbol{\mu}^{\mathrm{T}}\mathbf{u}^{*}\,\mathrm{d}\Gamma^q, \\ &\quad \forall\{\mathbf{u},\boldsymbol{\mu}\}\in\mathcal{D}_{\Theta}, \quad (20)\end{aligned}$$

defined on an admissible set

$$\begin{aligned}\mathcal{D}_{\Theta} &= \left\{\mathbf{u}^{*}(\mathbf{y})=\mathbf{0}, \quad \forall\mathbf{y}\in\Gamma_D^{\mathcal{UC}}\right\} \\ &\cap \left\{\mathbf{u}^{*}(\mathbf{y}) \text{ periodic}, \quad \forall\mathbf{y}\in\Gamma^{\mathcal{UC}}\right\} \\ &\times \left\{\boldsymbol{\mu}(\mathbf{y}), \quad \forall\mathbf{y}\in\Gamma^q,\ q=1,2,\ldots,r+1\right\}. \quad (21)\end{aligned}$$

C. Discretization

To convert the previous optimization problem to a finite-dimensional form, the fluctuating displacement fields $\mathbf{u}^{*}(\mathbf{y})$ are approximated, independently on each sub-domain, using a linear combination of basis functions stored in matrices $\mathbf{N}^q(\mathbf{y})$:

$$\mathbf{u}^{*}(\mathbf{y})\approx\tilde{\mathbf{u}}^{*}(\mathbf{y})=\mathbf{N}^q(\mathbf{y})\,\underline{\mathbf{u}}^{*q}, \quad \forall\mathbf{y}\in\Omega^q, \quad (22)$$

where

$$q=1,2,\ldots,r+1, \quad (23)$$

where $\underline{\mathbf{u}}^{*}$ denotes the unknown coefficients of linear combination. Next, we approximate the fluctuating strain employing the corresponding derivatives of the basis functions $\mathbf{N}^q(\mathbf{y})$ ordered in the geometric matrix $\mathbf{B}^q(\mathbf{y})$, see e.g. [2]:

$$\boldsymbol{\epsilon}(\mathbf{y})\approx\tilde{\boldsymbol{\epsilon}}(\mathbf{y})=\mathbf{B}^q(\mathbf{y})\,\underline{\mathbf{u}}^{*q}, \quad \forall\mathbf{y}\in\Omega^q, \quad (24)$$

where

$$q=1,2,\ldots,r+1. \quad (25)$$

The surface tractions are approximated using the values at the finite element nodal points via the identity

$$\int_{\Gamma^q}\boldsymbol{\mu}^{\mathrm{T}}\mathbf{u}^{*}\,\mathrm{d}\Gamma^q=\underline{\boldsymbol{\mu}}^{\mathrm{T}}\mathcal{L}^q\underline{\mathbf{u}}^{*q}, \quad (26)$$

where the matrix $\mathcal{L}^q$ ensures that the discretized displacement $\underline{\mathbf{u}}^{*q}$ is multiplied with the corresponding force $\underline{\boldsymbol{\mu}}$ acting at the same node and in the same direction. The discretized forces can be equivalently understood as the Lagrange multipliers arising from the nodal displacement continuity conditions.

Introducing the discretized fields into the energetic functional (20) results in the objective function

$$\begin{aligned}\tilde{\Theta} &= \frac{1}{2}\sum_{q=1}^{r+1}\int_{\Omega^q}\left(2\mathbf{E}^{\mathrm{T}}\mathbf{L}\mathbf{B}^q\underline{\mathbf{u}}^{*q}+\underline{\mathbf{u}}^{*q\mathrm{T}}\mathbf{B}^{q\mathrm{T}}\mathbf{L}\mathbf{B}^q\underline{\mathbf{u}}^{*q}\right)\mathrm{d}\Omega^q \\ &+ \underline{\boldsymbol{\mu}}^{\mathrm{T}}\mathcal{L}^1\mathbf{u}^{*1}-\sum_{q=2}^{r+1}\underline{\boldsymbol{\mu}}^{\mathrm{T}}\mathcal{L}^q\mathbf{u}^{*q}, \quad \forall\left\{\underline{\mathbf{u}}^{*q},\underline{\boldsymbol{\mu}}\right\}\in\mathcal{D}_{\tilde{\Theta}}, \quad (27)\end{aligned}$$

which is now a quadratic function defined on a finite-dimensional space $\mathcal{D}_{\tilde{\Theta}}=\mathbb{R}^n$.

D. Minimization of the objective function

First, we introduce the stiffness matrix

$$\mathbf{K}^q=\int_{\Omega^q}\mathbf{B}^{q\mathrm{T}}\mathbf{L}\mathbf{B}^q\,\mathrm{d}\Omega^q, \quad (28)$$

the right hand side vector

$$\mathbf{f}^q=-\int_{\Omega^q}\mathbf{E}^{\mathrm{T}}\mathbf{L}\mathbf{B}^q\,\mathrm{d}\Omega^q, \quad (29)$$

and change the sign of the matrix $\mathcal{L}^q$ for $q=2,3,\ldots,r+1$:

$$\mathcal{L}^q=-\mathcal{L}^q. \quad (30)$$

Because the matrices $\mathbf{B}^{q\mathrm{T}}\mathbf{L}\mathbf{B}^q$ are positive, the global minimum of the function $\tilde{\Theta}(\underline{\mathbf{u}}^{*},\underline{\boldsymbol{\mu}})$ coincides with the stationary point defined by the optimality conditions

$$\frac{\partial\tilde{\Theta}}{\partial\underline{\mathbf{u}}^{*q}}=\mathbf{0} \quad\Leftrightarrow\quad \mathbf{K}^q\underline{\mathbf{u}}^{*q}=\mathbf{f}^q-\mathcal{L}^{q\mathrm{T}}\underline{\boldsymbol{\mu}}, \quad (31)$$

where

$$q=1,2,\ldots,r+1, \quad (32)$$

and

$$\frac{\partial\tilde{\Theta}}{\partial\underline{\boldsymbol{\mu}}}=\mathbf{0} \quad\Leftrightarrow\quad \sum_{q=1}^{r+1}\mathcal{L}^q\underline{\mathbf{u}}^{*q}=\mathbf{0}. \quad (33)$$

E. Dual formulation

Now we proceed with expressing the fluctuating displacements $\underline{\mathbf{u}}^{*q}$ from the systems of equations (31) in the form

$$\underline{\mathbf{u}}^{*q}=\mathbf{K}^{q\dagger}\left(\mathbf{f}^q-\mathcal{L}^{q\mathrm{T}}\underline{\boldsymbol{\mu}}\right)+\mathbf{R}^q\underline{\boldsymbol{\alpha}}^q, \quad (34)$$

where

$$q=1,2,\ldots,r+1. \quad (35)$$

The first term $\mathbf{K}^{q\dagger}\left(\mathbf{f}^q - \mathcal{L}^{q\mathrm{T}}\underline{\boldsymbol{\mu}}\right)$ in relation (34) corresponds to the particular solution of the system (31), which is expressed by the help of the generalized inverse matrix $\mathbf{K}^{q\dagger}$ (see [4] or [5]) replacing the inverse matrix for singular $\mathbf{K}^q$. The second term $\mathbf{R}^q\underline{\boldsymbol{\alpha}}^q$ appearing in the relation (34) corresponds to a homogeneous solution of the system (31), expressed as the linear combination of rigid body motions $\mathbf{R}^q$ with coefficients of the linear combination $\underline{\boldsymbol{\alpha}}^q$.

Next, we substitute the fluctuating displacements $\underline{\mathbf{u}}^{*q}$ from relations (34) to system (33) and add the solvability conditions (37) to account again for a possible singularity of matrices $\mathbf{K}^q$:

$$\sum_{q=1}^{r+1}\mathcal{L}^q\mathbf{K}^{q\dagger}\mathcal{L}^{q\mathrm{T}}\underline{\boldsymbol{\mu}} - \sum_{q=1}^{r+1}\mathcal{L}^q\mathbf{R}^q\underline{\boldsymbol{\alpha}}^q = \sum_{q=1}^{r+1}\mathcal{L}^q\mathbf{K}^{q\dagger}\mathbf{f}^q, \quad (36)$$

$$\mathbf{R}^{q\mathrm{T}}\left(\mathbf{f}^q - \mathcal{L}^{q\mathrm{T}}\underline{\boldsymbol{\mu}}\right) = \mathbf{0}, \text{ where } q = 1, 2, \ldots, r+1. \quad (37)$$

Elimination of the primary unknowns $\underline{\mathbf{u}}^{*q}$ in (31–33) leads to a dual problem, formulated in terms of $\underline{\boldsymbol{\mu}}$ and $\underline{\boldsymbol{\alpha}}^q$. This problem can be efficiently solved using the Modified Conjugate Gradient (MCG) method, augmented by the projection step to ensure the solvability condition (37), see [4], [5] for further details.

F. Perfect bonding and perfect debonding of constituents

Due to its dual character, the FETI method offers an easy control of constituents' debonding in terms of nodal forces on the interface. In the actual implementation, the loading via the macroscopic strains is applied incrementally, such that the $\mathcal{UC}$ can relax the accumulated energy on the interface. For each step, an outer loop related to a given increment is executed. At the beginning of a loop, initial conditions of all the interfaces (e.g. the perfect bonding of constituents) are prescribed. Next, we load the $\mathcal{UC}$ and compute the actual values of interfacial forces using the MCG algorithm. If a force exceeds a given limit (i.e. the normal and tangential limit strengths R^n and R^t), then the debonding of the constituents is activated at the node. These steps are repeated until a convergence criterion is met. Note that if no compressive force limit in the normal direction is prescribed, the algorithm automatically reproduces the contact behavior between individual phases.

The perfect debonding of constituents can be prescribed in two fundamental ways. First, because the forces $\underline{\boldsymbol{\mu}}$ at the debonded nodes are equal to zero (and hence they are known), they can be eliminated from systems of equations (36–37). Second, we can directly modify the matrix $\mathcal{L}^q$. The first approach is employed in the numerical examples reported below.

G. Boundary conditions

The periodic boundary conditions are imposed with the aid of both kinematic and static boundary conditions. The periodic kinematic boundary conditions influence only the degrees of freedom located on the part of boundary belonging to the matrix and are imposed using the identical code numbers. For the rest of the boundary, the anti-periodic static boundary conditions are prescribed using the Lagrange multipliers, i.e. following the same procedure as for the case of perfect bonding at the constituents' interfaces.

IV. NUMERICAL EXPERIMENTS

In this section we show some numerical experiments obtained using an in-house code implemented in MATLAB 7.1. All reported examples were executed on one of the unit cells appearing in Fig. 2.

A. Controlled perfect debonding of constituents

In this experiment, we compare the macroscopic stress $\boldsymbol{\Sigma}$ computed using the FETI method with the results available in [8], corresponding to the hexagonal $\mathcal{UC}$ shown in Fig. 2a. Both plane stress and plane strain assumptions were used in the analysis to provide a comparison with a three-dimensional simulation [8]. The unit cell with 40% of fibers ($p = 0.4$) and material data

$$\begin{array}{rclcrcl} E^1 & = & 88\,\mathrm{GPa} & & E^{2,3,\ldots,6} & = & 200\,\mathrm{GPa} \\ \nu^1 & = & 0.299 & \text{and} & \nu^{2,3,\ldots,6} & = & 0.222 \end{array}, \quad (38)$$

were used. Note that E^i and ν^i denote the Young modulus and the Poisson ratio of the i-phase, respectively.

The $\mathcal{UC}$ was loaded by three elementary load cases

$$\mathbf{E} = [1,0,0]^{\mathrm{T}}, \quad \mathbf{E} = [0,1,0]^{\mathrm{T}}, \quad \mathbf{E} = [0,0,1]^{\mathrm{T}}, \quad (39)$$

and the corresponding macroscopic stress $\boldsymbol{\Sigma}$ was computed to arrive at the effective stiffness matrix $\mathbf{L}^{\mathrm{ef}}$. The resulting dependence of the effective stiffness matrix on the debonding angle α appears in Fig. 3a. The dashed line and the dot-and-dashed line display the results computed for the plane strain and the plane stress, respectively. The continuous line represents the results from article [8] (i.e. the three-dimensional $\mathcal{UC}$). Note that all data correspond to the case *without* contact conditions, i.e. the individual constituents can overlap freely. Evidently, very good match between reference results and the FETI-base procedure has been achieved. Moreover, it can be seen that the plane strain response provides an upper bound to the three-dimensional response, while the plane stress conditions result in a lower bound.

To further illustrate the influence of the contact condition between the individual constituents, the $\mathcal{UC}$ was loaded by the shear macroscopic strain

$$\mathbf{E} = [0,0,0.2]^{\mathrm{T}}. \quad (40)$$

The deformed shapes of the unit cells are compared in Fig. 4; Fig. 3b offers additional quantitative comparison between the two cases. The dashed and continuous lines in Fig. 3b denote the results with and without activation of the contact. The FETI-based algorithm correctly prevents the interpenetration of individual phases, see Fig. 4b, which leads to slightly more stiff shear response and to the appearance of additional normal stresses when compared with the former approach.

B. Load induced complete debonding of constituents

Finally, Fig. 5 plots the macroscopic stress-strain curves, determined for the composite shown in Fig. 2b in the plane stress state, subject to the macroscopic deformation

$$\mathbf{E} = [0.2,0,0]^{\mathrm{T}}. \quad (41)$$

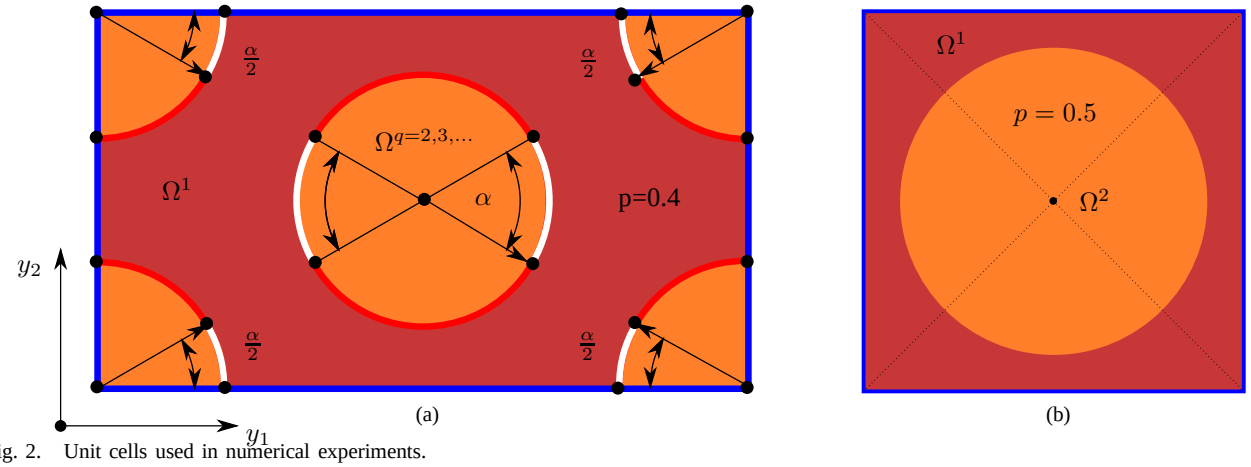

Fig. 2. Unit cells used in numerical experiments.

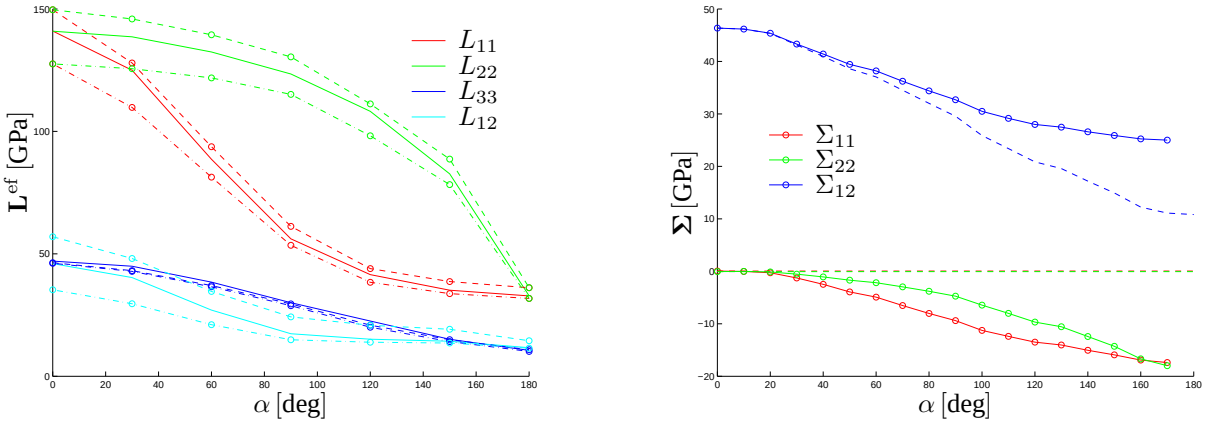

(a) Effective stiffness matrix $\mathbf{L}^{\mathrm{ef}}$.

(b) The contact problem.

Fig. 3. Dependence on the overall response on the debonding angle α.

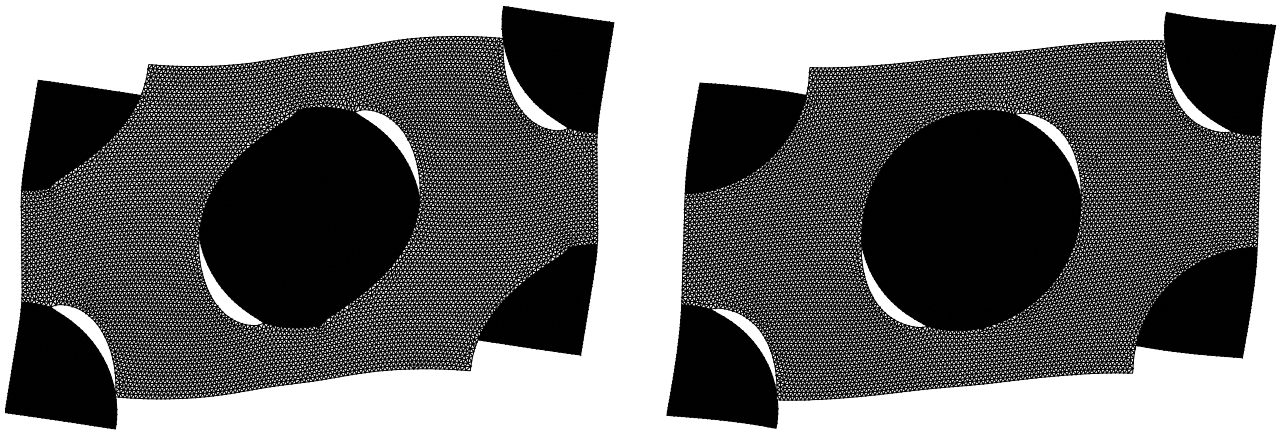

(a) Without the application of contact problem.

(b) With the application of contact problem.

Fig. 4. Overall deformation of $\mathcal{UC}$.

The following material data are used in the simulation

$$E^1 = 100\,\mathrm{GPa} \quad \nu^1 = 0.4 \quad \text{and} \quad E^2 = 500\,\mathrm{GPa} \quad \nu^2 = 0.2. \tag{42}$$

The continuous line and dotted lines, appearing in Fig. 5, display the normal macroscopic stress $\boldsymbol{\Sigma}$ in the direction of the nonzero macroscopic deformation $\mathbf{E}$ and orthogonal direction of the nonzero macroscopic deformation $\mathbf{E}$ respectively. Recall that in Fig. 5, R^n and R^t denote the normal and the tangential strength, respectively; the symbol j stands for a unit of length. It can be seen that the proposed numerical method is

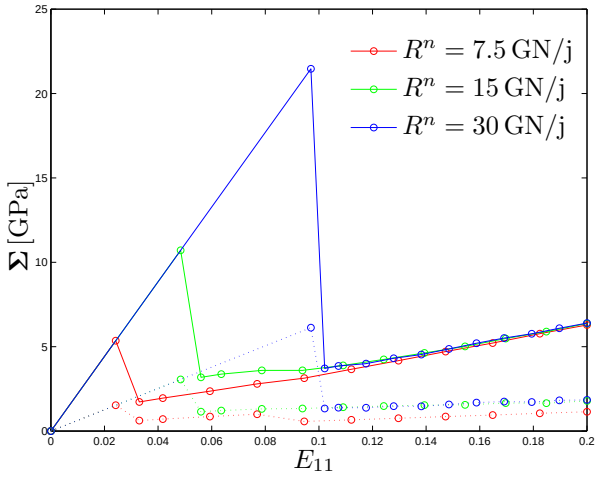

(a) $R^t = 30\,\mathrm{GN/j}$

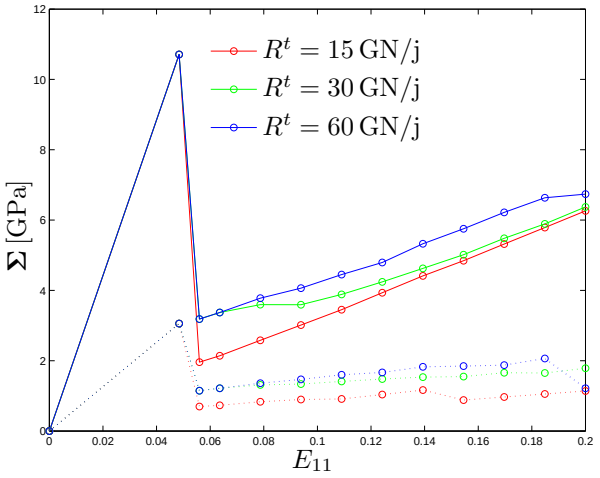

(b) $R^n = 15\,\mathrm{GN/j}$

Fig. 5. Stress-strain diagrams.

able to capture the complex interaction between the debonding and the inter-phase contact; a mechanism which is notoriously difficult to capture by existing analytical approaches of the continuum mechanics.

V. Conclusion

In the current work, a brief overview of a FETI-based procedure for the homogenization of composite materials developed in [4] has been presented. The most important conclusions can be summarized as follows:

- The proposed numerical scheme is very efficient in handling the problems, which are difficult to be treated by the displacement-based FEM approaches such as the non-penetration of individual phases and traction-based interfacial constitutive laws.
- The method is fully capable of capturing complex non-linear response typical of heterogeneous materials.

In the current state, the method is limited to specific, quite simplistic, constitutive laws for the interfacial region. Moreover, to fully assess the added value of the duality-based approach, more extensive comparison with the existing micromechanical methods should be performed. These topics are currently under investigation and will be reported separately.

Acknowledgment

Financial support of this work provided by the Grant Agency of the Czech Republic, projects GAČR 106/08/1379 and GAČR 106/07/1244, is gratefully acknowledged.

References

[1] M. Brdička, L. Samek, and B. Sopko. *Continuum mechanics*, 3rd ed. Academia, 2005, (In Czech).

[2] Z. Bittnar and J. Šejnoha. *Numerical methods in structural engineering*. ASCE Press, 1996.

[3] Z. Dostál, D. Horák, and O. Vlach. *FETI-based algorithms for modelling of fibrous composite materials with debonding*. Mathematics and Computers in Simulation, 76: 57–64, 2007.

[4] P. Gruber. *Homogenization of composite materials with imperfect bonding of constituents*. Diploma thesis, Czech Technical University in Prague, Praha, 2007, (In Czech). available online at http://mech.fsv.cvut.cz/~grubepav/download/gruber_master_thesis.pdf

[5] J. Kruis. *Domain Decomposition Methods for Distributed Computing*. Saxe-Coburg Publications, Kippen, Stirling, Scotland, 2006.

[6] J. Kruis and Z. Bittnar. *Reinforcement-matrix interaction modelled by FETI method*, in 17th International Conference on Domain Decomposition Methods. Linz: Johann Radon Institute for Computational and Applied Mathematics, 2006.

[7] J. C. Michel, H. Moulinec, and P. Suquet. *Effective properties of composite materials with periodic microstructure: A computational approach*. Computer Methods in Applied Mechanics and Engineering, 172: 109–143, 1999.

[8] M. Šejnoha and M. Srinivas, *Modeling of effective properties of composites with interfacial microcracks using PHA model*. Building Research Journal, 46: 99–108, 1998.

[9] O. Vlach, *Modeling of composites using duality-based solvers*. Diploma thesis. VSB-Technical University of Ostrava, Ostrava, 2001. available online at http://www.am.vsb.cz/index.php?lang=cz&menu=teaching&submenu=9